SIAM J. SCI. COMPUT.
Vol. 25, No. 3, pp. 857–880

A PHASE ERROR ANALYSIS OF MULTIGRID METHODS FOR HYPERBOLIC EQUATIONS*

W. L. WAN† AND TONY F. CHAN‡

Abstract. In this paper, we study the effects of the coarse grid correction process on multigrid convergence for hyperbolic problems in one and two dimensions. We approach this from the perspective of phase error, which allows us to exploit the hyperbolic nature of the underlying PDE. In particular, we consider three combinations of coarse grid operators and coarse grid solution approaches: (1) inexact coarse grid solve with direct discretization, (2) exact coarse grid solve with direct discretization, and (3) exact coarse grid solve with Galerkin coarse grid operator. For all these approaches, we show that the convergence behavior of multigrid can be precisely described by the phase error analysis of the coarse grid correction matrix, and we verify our results by numerical examples in one and two dimensions.

Key words. multigrid, hyperbolic equations, phase error, Fourier analysis

AMS subject classifications. 65F10, 65M12, 65M55, 65T50

DOI. 10.1137/S106482750240933X

1. Introduction.

Multigrid has been established as a powerful and successful numerical technique for fast solution of elliptic partial differential equations (PDEs). Many different approaches have been proposed and various sophisticated techniques have been developed for the cases of nonsmooth coefficient PDEs, complex geometries, and unstructured meshes (see, for example, [3, 17, 31, 35] and the survey in [12]). For the elliptic case, multigrid convergence is governed by smoothing of the high frequency errors and coarse grid correction of the low frequency errors. Classical Fourier analysis [3, 17, 35] and finite element analysis [2, 17, 37] have been well developed for the elliptic case. However, this elliptic multigrid principle may not hold for the hyperbolic case since the success of the standard techniques often rely on the intrinsic properties of elliptic PDEs, for instance, symmetry, decay of Green's function, and dissipation, which are not generally properties of hyperbolic problems.

Several smoothing techniques have been proposed for convection dominated problems. One approach is to apply Gauss–Seidel smoothing with the so-called downwind ordering [1, 10, 18, 24, 34]. Another approach is to use time-stepping methods as smoothers [19, 20, 23, 27]. The idea is that the smoothers not only reduce the high frequency errors but, more importantly, also propagate the errors along the flow directions. For the latter, the solution on the coarsest grid is done by a few smoothing steps. Thus, the multigrid process can be interpreted as speeding up the wave propagation by taking larger time step sizes on the coarse grids. As a result, errors can be removed rapidly by propagating them out of the boundary. A roadmap of recent multigrid developments for nonelliptic PDEs can be found in [9].

Fourier analysis has been a useful tools for analyzing multigrid methods and, more generally, iterative methods [13]. A simplified but more generally applicable

*Received by the editors June 8, 2002; accepted for publication (in revised form) June 9, 2003; published electronically November 21, 2003.

http://www.siam.org/journals/sisc/25-3/40933.html

†Department of Computer Science, University of Waterloo, Waterloo, ON, Canada N2L 3G1 (jwlwan@math.uwaterloo.ca). This author was supported by the Natural Sciences and Engineering Research Council of Canada and was partially supported by NSF grant ACI-0072112.

‡Department of Mathematics, University of California at Los Angeles, Los Angeles, CA 90095-1555 (chan@math.ucla.edu). This author has been partially supported by the NSF under contracts ACI-0072112 and DMS-9973341.

version, the local mode analysis, can be obtained by considering an infinite grid, i.e., ignoring the boundary effect. It was first introduced to analyze multigrid smoothing and two-level analysis by Brandt [3] and was later extended in [5, 6, 7, 8]; see also [17, 30, 31, 35]. In the half-space mode analysis [4, 5, 6, 10], the boundary effect can also be studied. For nonelliptic problems, first differential approximation (FDA) analysis [4] is often used to analyze smooth components. In this analysis, the discrete differential operator is replaced by its FDA [38], and the intergrid transfer and smoothing operators are ignored. For a model convection-diffusion equation with very small diffusion coefficient, it has been shown in [4, 10, 11] that the two-level convergence factor is at best 0.5. Fourier analysis of multigrid methods for convection dominated problems can also be found in [16, 29, 35]. Although two-level analysis is often sufficient to determine convergence behavior, occassionally, three-level analysis is necessary [36].

In the classical Fourier analysis mentioned above, the asymptotic convergence rate of multigrid convergence is often measured by the spectral radius of the iteration matrix. For elliptic problems, the spectral radius has been found to be an accurate measure of asymptotic convergence rates. For hyperbolic problems, however, the eigenvalues of the iteration matrix of multigrid are in general complex. The spectral radius estimate would ignore the phase angle information. In the analysis of numerical schemes for hyperbolic equations, phase angle, more commonly known as phase velocity, has been used extensively [32]. However, the use of phase error analysis in the multigrid context has not been much explored. We are advocating such an approach in this paper. We use standard Fourier analysis to compute the Fourier symbol of the multigrid iteration matrix, in particular, the symbol of the coarse grid correction matrix. In addition to the spectral radius, we also study the phase error of the Fourier symbol to gain more insight into the multigrid convergence.

The discretization schemes studied in this paper are primarily first order and are commonly used in multigrid literature for hyperbolic or convection-diffusion equations (see, e.g., [10, 31, 36, 39]). However, our phase error analysis is general; it is not restricted to any particular scheme. In section 4.4, a nonlinear second order total vartiation diminishing scheme is considered. Although Fourier analysis is not applicable, we show numerically that the phase error analysis can still be used to analyze the effectiveness of the coarse grid correction. Furthermore, we remark that the discretization scheme alone does not determine the phase error of the coarse grid correction, which is a combination of restriction, coarse grid solution (CGS), and prolongation. For instance, although the dissipation of first order upwind schemes dominates the dispersive effect, we find that the phase error of the coarse grid correction process can still be significantly large. A change in the multigrid components such as restriction and prolongation, however, can reduce or even remove (cf. section 5) the phase error.

To explore the wave propagation nature of the underlying hyperbolic PDEs, Gustafsson and Lötstedt [15, 26] first analyze the phase error (or phase velocity) of a multigrid approach and prove that a speedup of $2^K - 1$ in convergence is obtained using K grids for smooth errors, which would not be inferred from the spectral radius analysis. In practice, however, the multigrid convergence can be much slower than the analysis predicts due to severe numerical oscillations generated by the algorithm (cf. section 2). In the analysis of Gustafsson and Lötstedt, they focus primarily on the leading order term of the asymptotic expansion of the phase speed. In this paper, we extend their analysis to include also the first order correction term with which we

can explain the dispersive behavior of the multigrid process, which turns out to have a significant influence on the convergence rate.

We find that the phase error analysis is not only useful for the wave propagation multigrid approach but can also be used to explain the efficiency of other coarse grid correction methods. One common coarse grid correction approach is to use discretization matrices as coarse grid operators (CGOs). It has been shown by Brandt and Yavneh in [4, 10, 11, 39] that the resulting coarse grid correction has O(1) error for the characteristic components for 2D nonaligned flow problems. Our phase error analysis not only recovers the same result but also provides more insight into the source of the error. In particular, we prove that this coarse grid correction is only first order accurate for cross-characteristic components due to the phase shift error caused by the discretization CGOs.

In this paper, we show that the Galerkin coarse grid correction [28, 40] can be a more efficient approach (the same is also observed in [39]) from the perspective of the phase error. We prove that the phase error of the coarse grid correction is smaller than that of the previous approach, and hence higher order accuracy of the coarse grid correction can be achieved. We note, however, that Galerkin CGOs tend to become central difference discrete operators, which may lead to spurious oscillations in the coarser grid calculations. To remedy this problem, Dendy [14] uses operator-dependent restriction and interpolation constructed from the symmetric part of the operator. Yavneh [39] also uses interpolation and restriction operators, which depend on the flow directions, together with artificial viscosity. He also pointed out that the order of accuracy of the high frequency components is crucial to obtain efficient Gakerlin coarse grid correction. Based on our phase error analysis, one could use the Galerkin approach with an appropriately defined interpolation so that the Galerkin CGO is stable. How to construct such an interpolation, however, requires substantial investigation and is not within the scope of this paper. We also note that accurate (higher order) non-Galerkin CGOs can be constructed, which would result in small phase errors. However, such CGOs may have the same stability problem as the Galerkin approach. Thus, the non-Galerkin CGOs we considered are limited to those by direct discretization.

We would like to remark that the FDA analysis [4] does not take into account the effect of the intergrid transfer operators. However, as reported in [4, p. 84], downwind residual transfer is observed to produce better convergence results, which was not explained. In fact, different interpolation and restriction operators lead to very different phase errors of the coarse grid correction process. In section 5, we demonstrate how our phase error analysis can successfully prove the fast convergence of two multigrid methods using upwind-type interpolation and restriction.

In section 3, explicit analytic formulae for the asymptotic expansion of the phase error of the different coarse grid correction approaches are established in one dimension. In section 4, results in two dimensions are presented with emphasis on Fourier components in the characteristic and cross-characteristic directions. Numerical results are given in section 6 to compare how these coarse grid correction approaches affect the actual multigrid convergence. Finally, concluding remarks are given in section 7.

2. Model problem. The model problem we are interested in is the steady state solution of linear hyperbolic equations,

$$Lu(x) \equiv \sum_{i=1}^{d} a_i(x) \frac{\partial u}{\partial x_i} = f(x) \qquad x \in \Omega,$$

subject to periodic boundary conditions. Here, $a_i(x)$ are smooth functions, and Ω is a d-dimensional unit cube.

Discretizing the equation by finite difference methods on a standard uniform fine grid Ω^h on Ω with mesh size h results in a linear system

$$L^h u^h = f^h.$$

The discrete problem is solved using K grids, $\{\Omega^l\}_{l=0}^{K-1}$, where the finest grid is $\Omega^{K-1} = \Omega^h$, and Ω^{l-1} is obtained from Ω^l by standard full coarsening. Denote by p^l the prolongation operator from Ω^{l-1} to Ω^l and by r^l the restriction operator from Ω^l to Ω^{l-1}, $l = 1, 2, \ldots, K-1$. Also, denote the smoothing operator on Ω^l by $\mathcal{S}^l$, and denote q steps of smoothing by $\mathcal{S}_l^{(q)}$. The solution process on the coarsest grid is denoted by CGS. A standard multigrid V(q_1,q_2)-cycle algorithm with q_1 steps of presmoothing and q_2 steps of postsmoothing can be written as [3, 17]

```
procedure MG(l,u,f)
if l = 0
  u = CGS(u, f);
else
  u = S_l^(q1)(u, f);
  d = r^l(L^l u − f);
  v = 0;
  MG(l − 1, v, d);
  u = u − p^l v;
  u = S_l^(q2)(u, f);
end
  u = u^n;
  MG(K − 1, u, f);
  u^(n+1) = u;
```

Multigrid convergence is often studied by means of Fourier analysis [6, 7, 8, 17, 30, 31, 35]. In two dimensions, the discrete Fourier function (mode), $\psi^h_{\mu,\nu}$, can be written as

$$\psi^h_{\mu,\nu}(x^h_{j,k}) = \frac{1}{2} e^{i\mu\pi x^h_j} e^{i\nu\pi y^h_k}, \qquad -N \le \mu, \nu \le N-1.$$

We note that $\psi^h_{\mu,\nu}$, with $|\mu|$, $|\nu| \approx 0$, correspond to smooth or less oscillatory (low) modes whereas $\psi^h_{\mu,\nu}$, $|\mu|$, $|\nu| \approx N$, correspond to the most oscillatory (high) modes. The orthogonal Fourier transform matrix Q_h can be formed by taking $\psi^h_{\mu,\nu}$ as its columns. For two-grid analysis, it is customary to pair up the low-low, high-low, low-high, and high-high modes together:

$$Q_h = [\cdots \psi^h_{\mu,\nu}\ \psi^h_{\mu,\nu'}\ \psi^h_{\mu',\nu}\ \psi^h_{\mu',\nu'} \cdots],$$

where $\mu' = \mu - N$, $\nu' = \nu - N$. Denote the Fourier transform of a matrix B by $\hat{B} \equiv Q_h^{-1} B Q_h$, with entries $\hat{B}_{\mu,\nu}$.

The iteration matrix of the V(q_1,q_2)-cycle can be written as

$$M = S^{q_2} C S^{q_1},$$

where C and S are the coarse grid correction matrix and the iteration matrix of the smoother, respectively. Hence $\hat{M} = \hat{S}^{q_2} \hat{C} \hat{S}^{q_1}$. With the ordering used in the Fourier

transform and assuming PDE coefficients being constant, $\hat{M}$ is a block diagonal matrix with each block a 4×4 matrix $\hat{M}_{\mu,\nu}$, where

$$\hat{M}_{\mu,\nu} = \hat{S}^{q_2}_{\mu,\nu} \hat{C}_{\mu,\nu} \hat{S}^{q_1}_{\mu,\nu}, \qquad \mu, \nu = -N/2, \ldots, N/2 - 1.$$

If the coarse grid problem is solved exactly, i.e., $CGS(u, f) = (L^H)^{-1} f$, then

$$\hat{C}_{\mu,\nu} = I - \hat{p}_{\mu,\nu} (\hat{L}^H_{\mu,\nu})^{-1} \hat{r}_{\mu,\nu} \hat{L}^h_{\mu,\nu},$$

where p, r, and L^H are the prolongation, restriction, and CGOs, respectively.

The convergence of the two-grid method will then be determined by $\hat{M}_{\mu,\nu}$, which is often referred to as the Fourier symbol of the iteration matrix. In standard Fourier analysis of two-grid convergence, the spectral radius of $\hat{M}_{\mu,\nu}$ is considered. More precisely, the asymptotic convergence rate is often measured by (see, e.g., [17, 31, 35])

$$\rho := \sup_{-N/2 \le \mu,\nu \le N/2-1} \rho(\hat{M}_{\mu,\nu}),$$

where $\rho(\hat{M}_{\mu,\nu})$ denotes the spectral radius of $\hat{M}_{\mu,\nu}$. Since eigenvalues of $\hat{M}_{\mu,\nu}$ are complex in general, the spectral radius takes into account only the modulus information of the eigenvalues while ignoring the phase angle information. Using the terminology from numerical methods for solving hyperbolic equations, the spectral radius essentially corresponds to the dissipation and the phase angle corresponds to the dispersion. Their definitions are given as follows.

Given a finite difference scheme in one dimension, suppose the Fourier transform of the numerical solution at time step $n + 1$ can be written as

$$\hat{u}^{n+1}(\mu) = g(\mu) \hat{u}^n(\mu),$$

where $g(\mu)$ is the amplification factor and μ is the wave number. The scheme is dissipative if $|g(\mu)| < 1$, and dispersive if the phase velocity [32], $\kappa(\mu)$, defined as,

$$\kappa(\mu) \equiv -\frac{\arg(g(\mu))}{\mu \pi \Delta t},$$

is different for a different wave number μ, where Δt is the time step size. The phase velocity, $\kappa(\mu)$, measures the propagation speed of the wave with wave number μ.

The concepts of dissipation and dispersion become very useful in the context of multigrid when one interprets the smoothing process as solving a pseudotime-dependent problem:

$$\frac{\partial u^l}{\partial t} + L^l u^l = f^l, \qquad l = 0, 1, \ldots, K - 1. \tag{2.1}$$

The coarse grid problem is often solved by a few steps of smoothing, e.g., $CGS(u, f) = \mathcal{S}^{q_1+q_2}(u, f)$. This approach was proposed by Jameson, Schmidt, and Turkel [19, 21] and Ni [27] and later analyzed by Gustafsson and Lötstedt [15, 26]. The idea is to accelerate error propagation by taking larger time steps on the coarse grids. To give a more precise account of the wave propagation property of the multigrid V(1,0)-cycle, Gustafsson and Lötstedt analyzed the dispersion, or phase velocity, of the multigrid process by a Fourier analysis of the two-grid iteration matrix $M = CS$. The smoother

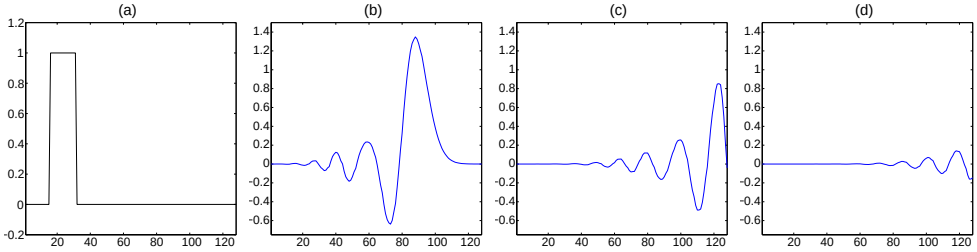

FIG. 2.1. *The numerical solutions given by a three-level multigrid V-cycle at* (a) *iteration* = 0, (b) *iteration* = 20, (c) *iteration* = 40, (d) *iteration* = 60.

considered is an m-stage Runge–Kutta method, and hence the coarse grid correction matrix, C, and the iteration matrix of the smoother, S, are given by

$$C = I + \sum_{j=1}^{m} \Delta t_H^j p (L^H)^{j-1} \prod_{k=m-j+1}^{m} (-\alpha_k) r L^h,$$

$$S = I - \sum_{j=1}^{m} (\Delta t_h L^h)^j \prod_{k=m-j+1}^{m} \alpha_k,$$

where $\alpha_k' s$ are parameters of the m-stage Runge–Kutta method. We summarize the results of the analysis of Gustafsson and Lötstedt in one dimension as follows.

THEOREM 2.1. *Let λ_1 be the first eigenvalue of $\hat{M}_\mu$. For frequency $\mu \approx 0$,*

$$\lambda_1(\mu) = 1 - (\Delta t_h + \Delta t_H) i \mu \pi + O(\mu^2).$$

Consequently, the phase velocity of the two-grid method is

$$\kappa(\mu) = -\frac{\arg(\lambda_1(\mu))}{\mu \pi \Delta t_h} = 1 + \frac{\Delta t_H}{\Delta t_h} = 3.$$

In general, if t_l denotes the time step on grid l, then the phase speed of the K-level multigrid method is given by

$$\kappa(\mu) = \frac{1}{\Delta t_1} \sum_{j=1}^{K} \Delta t_j = 2^K - 1, \qquad \mu \approx 0.$$

Thus, they can explain the fast propagation of this multigrid approach, which would not be explained by the standard spectral radius or dissipation analysis.

However, the effective speed of wave propagation observed is much slower than the analysis predicts. The reason is that their analysis focuses primarily on the leading order terms of the Taylor expansion of λ_1, which only accounts for the speed of propagation of smooth waves. However, the error after smoothing also consists of nonnegligible higher frequency modes, which need to be taken into account.

As an example, we take a square wave as the initial error, which consists of nonnegligible high frequency Fourier modes. Snapshots of the error in the first sixty multigrid V-cycles are shown in Figure 2.1. We use linear interpolation, one step of Euler smoothing, and three coarse grids. The number of fine grid points is 128. For $\Delta t = 0.5 \Delta x$, the single grid method (i.e., only smoothing) will converge in 256 iterations. The analysis of Gustafsson and Lötstedt estimated that the multigrid

method should have a speedup of $2^3 - 1 = 7$, and it should have converged in 36 iterations. However, it takes more than 100 iterations to reduce the initial residual norm by 10^{-6}. The reason is that, as shown in Figure 2.1, oscillations are generated as the wave propagates to the right—a phenomenon of dispersion.

In this paper, we do not consider any specific smoothers; we only assume that the smoothers are effective in reducing high frequency errors. Thus the multigrid convergence will hinge on the effectiveness of the coarse grid correction. As the main theme of this paper, we shall consider three types of coarse grid correction approaches commonly used in the literature and analyze them using phase error analysis. The first one is the wave propagation approach just described in which the coarse grid problem is solved approximately by a few smoothing steps and the CGO is obtained by direct discretization. The second approach is to solve the coarse grid problem exactly and also obtain the CGO by direct discretization. The third approach is like the second one except that Galerkin CGO is used.

3. One dimension. This paper will focus on the phase error analysis in two dimensions. However, most of the 2D results are motivated by the 1D analysis. To make the paper self-contained, we briefly summarize the main 1D results here. The details of the analysis can be found in [33]. The 1D hyperbolic equation is discretized by the standard first order upwinding. We note that a higher order method can also be considered (cf. section 4.4). In this paper, however, the primary focus is on the phase error analysis of the coarse grid correction process, which is the result of the restriction, CGO, and interpolation.

3.1. Inexact coarse grid solve, direct discretization CGO. In the Fourier analysis of Gustafsson and Lötstedt [15, 26] for this approach, they only provide information on the phase speed of the smooth wave propagation. Thus, their analysis would not be able to explain the oscillatory phenomenon as shown in Figure 2.1. In this section, we extend the phase velocity analysis to also include the first order term in the asymptotic expansions.

The coarse grid solve is carried out by one step of m-stage Runge–Kutta smoothing. For easy exposition, we take $m = 1$, $\Delta t_H = \lambda H$, where λ is the CFL-number. Thus the coarse grid correction matrix can be written as

$$C = I - \lambda H p r L^h,$$

where p is the linear interpolation and $r = \frac{1}{2}p^T$ its transpose, as considered in [15, 26]. Then, the 2×2 subblocks of the Fourier transform of C are given by

$$\begin{aligned} \hat{C}_\mu &= I - \lambda H \hat{p}_\mu \hat{r}_\mu \hat{L}_\mu^h \\ &= I - \lambda H \begin{bmatrix} c_\mu^2 \\ -s_\mu^2 \end{bmatrix} \begin{bmatrix} c_\mu^2 & -s_\mu^2 \end{bmatrix} \frac{1}{h} \begin{bmatrix} 1 - e^{-\mu\pi hi} & 0 \\ 0 & 1 + e^{-\mu\pi hi} \end{bmatrix}. \end{aligned} \tag{3.1}$$

Since Gustafsson and Lötstedt consider one presmoothing and no postsmoothing, the Fourier symbol of the iteration matrix has the form $\hat{M}_\mu = \hat{C}_\mu \hat{S}_\mu$. Note that $\hat{S}_\mu$ is a diagonal matrix. Moreover, if the smoother is effective in reducing high frequency errors, then $\hat{S}_\mu(1,1)$, the (1,1) entry of $\hat{S}_\mu$, is dominant. Consequently, $\hat{M}_\mu$ is essentially determined by $\hat{C}_\mu(1,1)$, which represents the low frequency–low frequency interaction. In other words, it represents how the smooth waves are changed by the coarse grid correction. Hence, we focus just on the (1,1) entry of $\hat{C}_\mu$. By (3.1),

$$\hat{C}_\mu(1,1) = 1 - 2\lambda c_\mu^4 (1 - e^{-\mu\pi hi}) \equiv |\hat{C}_\mu(1,1)| e^{-i\kappa(\mu)\mu\pi h\lambda}.$$

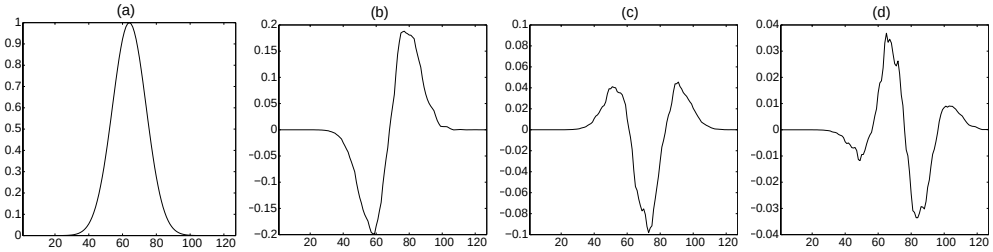

FIG. 3.1. *The numerical solutions given by a four-level multigrid with exact coarse grid solve at* (a) *iteration* = 0, (b) *iteration* = 1, (c) *iteration* = 2, (d) *iteration* = 3.

Below we present our result on the dispersion of $\hat{C}_\mu(1,1)$, which is not considered explicitly by Gustafsson and Lötstedt [15].

THEOREM 3.1. *The coarse grid correction is dissipative of order* 2 *for* $0 < \lambda \le 1/2$ *and dispersive. More precisely, the dissipation and phase velocity of* $\hat{C}_\mu$ *are given, respectively, by*

$$|\hat{C}_\mu(1,1)| \le 1 \qquad \textit{if and only if} \qquad 0 < \lambda \le \frac{1}{2},$$

$$\kappa(\mu) = 2 + \frac{8\lambda - 15}{12}(\mu\pi h)^2 + O(\mu\pi h)^4.$$

Proof. For the proof see [33]. □

There are two implications of Theorem 3.1. First, considering $|\hat{C}_\mu(1,1)|$, the CFL condition on λ ($\le \frac{1}{2}$) is more restrictive than that imposed by Euler's smoothing ($\lambda \le 1$). Second, the leading order term shows that the coarse grid correction has an effect of propagating smooth waves with speed 2. Furthermore, we note that the second term is negative for $0 < \lambda < 1$. Thus, the nonconstant smooth waves will have a negative phase velocity error, which accounts for the oscillations generated at the tail as the wave propagates to the right; see Figure 2.1.

3.2. Exact coarse grid solve, direct discretization CGO. The dispersion effect discussed in section 3.1 is largely due to the inexact coarse grid solve, and it explains that different waves travel at different speeds, which delay the overall multigrid convergence. In this section, we consider an exact coarse grid solve instead. Thus, as in standard multigrid, the idea is to eliminate the smooth errors completely on the coarse grid while the oscillatory errors are damped by the smoother. The CGOs used are the same as before; we apply the same discretization scheme to all the coarse grids. Linear interpolation is used for intergrid transfer. As an example, we apply this multigrid with three coarse grids to solve our model problem. The numerical solutions obtained are shown in Figure 3.1. Although the solutions are converging to 0 (note the change in scale on the y-axis), the formation of the relatively large error in the middle is unexpected since the starting solution is very smooth, and the exact coarse grid solve should, in principle, have eliminated it completely.

We discuss the numerical oscillation with the help of several plots, followed by a phase error analysis. We use the same multigrid method to solve the model problem. This time, we use three grids and many smoothing steps (25, and $\lambda = 0.8$) to provide a better illustration. In Figure 3.2(a), we start with a smooth starting function $u^{(1)}$ (solid line) on the first grid and obtain $\bar{u}^{(1)}$ (dashed line) after 25 smoothing steps. We then restrict the residual to the second grid and apply the two-grid method to solve the error equation on this grid. The initial guess is zero. The initial error,

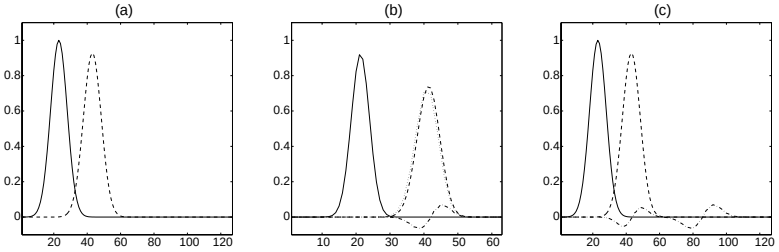

FIG. 3.2. *The initial error (solid line), error after smoothing (dashed line), error from coarse grid correction (dotted line), error after coarse grid correction (dash-dotted line) on* (a) *first grid,* (b) *second grid,* (c) *first grid.*

$e^{(2)}$ (solid line), and the error after 25 smoothing steps, $\bar{e}^{(2)}$ (dashed line), are shown in Figure 3.2(b). We then restrict the residual to the third grid and solve the error equation exactly. The coarse grid error is then interpolated back to the second grid as $pe^{(3)}$ (dotted line) in Figure 3.2(b). In principle, the coarse grid error $pe^{(3)}$ should approximate well the error on the current grid $\bar{e}^{(2)}$, which seems to be close, but it is clearly shifted a bit to the left. Thus, after the coarse grid correction, the error of the updated solution (dash-dotted line) shows an oscillation underneath $\bar{e}^{(2)}$ due to the shift. Finally, we interpolate the solution on the second grid, which is the coarse grid error for the first grid, back to the first grid. The solution after the coarse grid correction (dash-dotted) is shown in Figure 3.2(c). Instead of obtaining a near zero function, we have two oscillations corresponding to the coarse grid corrections of the second and third grids, respectively.

We use a phase error analysis to explain this phenomenon for the two-grid method. With exact coarse grid solve, the coarse grid correction matrix is

$$C = I - p(L^H)^{-1} r L^h.$$

As in the previous approach, we are interested in the low-low interaction, i.e., the (1,1) entry of $\hat{C}_\mu$.

THEOREM 3.2. *The coarse grid correction of smooth waves given by the exact coarse grid solve together with linear interpolation is only first order accurate, with*

$$|\hat{C}_\mu(1,1)| = \frac{\mu\pi h}{2} + O(\mu\pi h)^2.$$

Proof. We first consider the term $D \equiv p(L^H)^{-1} r L^h$, i.e., the effect of exact coarse grid solve. The (1,1) entry of $\hat{D}_\mu$ can be calculated as

$$\hat{D}_\mu(1,1) = \frac{2c_\mu^4}{1 + e^{-\mu\pi hi}} = c_\mu^4 + i s_\mu c_\mu^3 = c_\mu^3 e^{\mu\pi hi/2}.$$

As a result,

$$\hat{C}_\mu(1,1) = 1 - \hat{D}_\mu(1,1) = 1 - c_\mu^3 e^{\mu\pi hi/2}.$$

The results follow by Taylor expansion. ∎

By examining the formula of $\hat{D}_\mu(1,1)$, we can see that $\hat{D}_\mu(1,1)$ has the effect of shifting waves of any frequency by 1/2 grid point (to the left) immediately after the exact coarse grid solve. In other words, the coarse grid error given by the exact

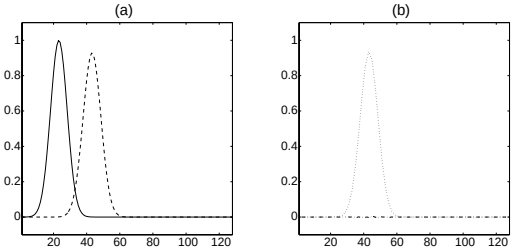

FIG. 3.3. (a) *The initial error (solid line) and error after smoothing (dashed line),* (b) *The error from coarse grid correction (dotted line) and error after coarse grid correction (dash-dotted line) on the first grid.*

coarse grid solve and the fine grid error differ by 1/2 grid point. Thus, it explains precisely the slight shift of the coarse grid correction error (dash-dotted line) shown in Figure 3.2(b). As we shall see in the next section, this shift arises essentially from the discretization of the first order PDE with two different mesh sizes, which cause dispersion to occur. Due to the shift generated by $\hat{D}_\mu(1,1)$, the amplification factor of $\hat{C}_\mu(1,1) = O(\mu\pi h)$, i.e., the coarse grid correction, is only first order accurate.

3.3. Exact coarse grid solve, Galerkin CGO. In the elliptic case, one often uses the Galerkin approach to form the coarse grid correction operator

$$G^H = rL^h p,$$

since the coarse grid error is minimized in the A-norm. For hyperbolic equations, however, the Galerkin CGO is less commonly used. In this section, we consider the use of a Galerkin CGO with exact coarse grid solve and show that it does not have the dispersion effect caused by the discretization matrix on the coarse grid, as in the non-Galerkin approach.

We start with a similar numerical experiment as in the previous section. This time, we only use two grids. In Figure 3.3(a), it shows the smooth starting function and the solution after 25 smoothing steps. An exact coarse grid solve is used with a Galerkin CGO. The interpolated coarse grid error (dotted line) and the error after coarse grid correction (dash-dotted line) are shown in Figure 3.3(b). We see that the CGS approximates well the error on the fine grid, and hence the error after the coarse grid correction is essentially gone; thus, there is no visible oscillation.

We explain the numerical observation by the phase error analysis. Since the CGO is obtained by the Galerkin process, its Fourier transform can be calculated as follows:

$$\hat{G}^H_\mu = \hat{r}_\mu \hat{L}^h_\mu \hat{p}_\mu = \frac{\cos^2(\mu\pi h) - e^{-2\mu\pi hi}}{2h}.$$

THEOREM 3.3. *The coarse grid correction of smooth waves given by the exact coarse grid solve and Galerkin CGO is third order accurate, with*

$$|\hat{C}_\mu(1,1)| = \frac{1}{8}(\mu\pi h)^3 + O(\mu\pi h)^5.$$

Proof. We define D as in the proof of Theorem 3.2. The (1,1) entry of $\hat{D}_\mu$ is then given by

$$\hat{D}_\mu(1,1) \equiv \hat{p}_\mu(\hat{G}^H_\mu)^{-1}\hat{r}_\mu\hat{L}^h_\mu = \frac{2c^4_\mu(1 - e^{-\mu\pi hi})}{\cos^2(\mu\pi h) - e^{-2\mu\pi hi}} = \frac{c^3_\mu}{c^6_\mu + s^6_\mu}(c^3_\mu + is^3_\mu).$$

By direct calculation, the amplification factor of $\hat{D}_\mu(1,1)$ and the phase angle θ are given by

$$|\hat{D}_\mu(1,1)| = \frac{c_\mu^3}{\sqrt{c_\mu^6 + s_\mu^6}}, \qquad \theta(\mu\pi h) = \arctan\left(\frac{s_\mu^3}{c_\mu^3}\right) = \frac{1}{8}(\mu\pi h)^3 + O(\mu\pi h)^5.$$

The results for $\hat{C}_\mu$ follow by Taylor expansion. ∎

We see that the phase error of $\hat{D}_\mu(1,1)$ in the Galerkin approach is two orders of magnitude smaller than that in the non-Galerkin approach, implying that essentially no shifting occurs after the exact coarse grid solve. Consequently, the coarse grid correction operator is two orders more accurate.

4. Two dimensions. We extend the phase error analysis of section 3.1 to two dimensions. Consider the convection dominated problem on a unit square:

$$-\epsilon\Delta u + a(x,y)u_x + b(x,y)u_y = f, \qquad x \in \Omega = (-1,1)\times(-1,1),$$

with periodic boundary condition. In particular, we focus on two model problems:

(1) entering flow (constant coefficient):

$$a(x,y) \equiv a, \quad b(x,y) \equiv b.$$

(2) recirculating flow (variable coefficient):

$$a(x,y) = 4x(x-1)(1-2y), \quad b(x,y) = -4y(y-1)(1-2x).$$

We discretize the equation using the first order upwind scheme on a uniform fine grid $\{(x_j^h, y_k^h)\}_{-N\le j,k\le N-1}$ with mesh size h, resulting in a linear system

$$L^h u^h = f^h,$$

where

$$\begin{aligned}(L^h u^h)_{i,j} = \epsilon&\frac{4u_{i,j}^h - u_{i-1,j}^h - u_{i+1,j}^h - u_{i,j-1}^h - u_{i,j+1}^h}{h^2}\\ &+\frac{(-a-|a|)u_{i-1,j}^h + 2|a|u_{i,j}^h + (a-|a|)u_{i+1,j}^h}{2h}\\ &+\frac{(-b-|b|)u_{i,j-1}^h + 2|b|u_{i,j}^h + (b-|b|)u_{i,j+1}^h}{2h};\end{aligned}$$

see, for instance, [39]. Since our primary focus is on the limit $\epsilon \to 0$, we shall ignore the elliptic term in the analysis. Also, we assume a, b are positive; general a, b can be treated similarly.

We remark that Gauss–Seidel smoothing with "downstream ordering" is often used in multigrid for convection dominated problems [1, 10, 18, 24, 34]. In this approach, the role of Gauss–Seidel is not only as a smoother but also, at least in part, as a solver. In this paper, however, we concentrate only on the effect of coarse grid correction, and hence we do not take into account the ordering issue.

4.1. Inexact coarse grid solve, direct discretization CGO. In the 1D analysis, we conclude that the multigrid V-cycle convergence is delayed by the oscillation generated as a result of the dispersive effect caused by the coarse grid correction. In the following, we shall show that similar oscillations occur also in the 2D case. The interpolation, p, and the restriction, r, are bilinear and full weighting, respectively; hence $r = 1/4p^T$. The smoother is the same as in one dimension—a first order Runge–Kutta method, which is also Richardson smoothing.

Assuming a, b constant, the Fourier symbol of the coarse grid correction matrix C is given by

$$\begin{aligned}\hat{C}_{\mu,\nu} &= I - \lambda H \hat{p}_{\mu,\nu} \hat{r}_{\mu,\nu} \hat{L}^h_{\mu,\nu} \\ &= I - 2\lambda h \begin{bmatrix} c_\mu^2 c_\nu^2 \\ -s_\mu^2 c_\nu^2 \\ -c_\mu^2 s_\nu^2 \\ s_\mu^2 s_\nu^2 \end{bmatrix} \begin{bmatrix} c_\mu^2 c_\nu^2 & -s_\mu^2 c_\nu^2 & -c\mu^2 s_\nu^2 & s_\mu^2 s_\nu^2 \end{bmatrix} \hat{L}^h_{\mu,\nu}.\end{aligned}$$

In particular, we are interested in the (1,1) entry of $\hat{C}_{\mu,\nu}$,

$$\hat{C}_{\mu,\nu}(1,1) = 1 - 2\lambda h c_\mu^4 c_\nu^4 \left[\frac{a}{h}(1 - e^{-\mu\pi h i}) + \frac{b}{h}(1 - e^{-\nu\pi h i}) \right].$$

To gain more insight into the formula of $\hat{C}_{\mu,\nu}(1,1)$, we consider the special case where $a = b = 1$ and we have frequencies in the characteristic direction, i.e., $\nu = \mu$.

THEOREM 4.1. *Assume $a = b = 1$. In the characteristic direction, i.e., $\nu = \mu$, the coarse grid correction is dissipative for $0 < \lambda \le 1/4$, and dispersive, i.e.,*

$$|\hat{C}_\mu(1,1)| \le 1 \qquad \text{if and only if} \qquad 0 < \lambda \le \frac{1}{4},$$
$$\kappa(\mu) = 2 + \left(2\lambda - \frac{9}{4}\right)(\mu\pi h)^2 + O(\mu\pi h)^4.$$

Proof. Under the assumptions,

$$\begin{aligned}\hat{C}_{\mu,\nu}(1,1) &= 1 - 2\lambda h c_\mu^8 \left[\frac{2}{h}(1 - e^{-\mu\pi h i}) \right] \\ &= 1 - 2\lambda c_\mu^6 \sin^2(\mu\pi h) - i4\lambda c_\mu^8 \sin(\mu\pi h).\end{aligned}$$

The results follow from Taylor expansion on $|\hat{C}_{\mu,\nu}(1,1)|$ and phase of $\hat{C}_{\mu,\nu}(1,1)$. ∎

Figure 4.1(a) shows $\max_{\mu,\nu} |\hat{C}_{\mu,\nu}(1,1)|$ for different values of λ, $a = b = 1$. We note that the stability requirement for the coarse grid correction is $0 \le \lambda \le 1/4$, whereas that for smoothing is only $0 \le \lambda \le 1/2$. Thus, a more restrictive CFL-number is needed, which is consistent with the 1D result (cf. Theorem 3.1). For $\lambda = 0.25$, Figure 4.1(b) shows that $\hat{C}_{\mu,\nu}(1,1)$ is dissipative for all values of μ, ν. Figure 4.1(c) shows the phase velocity of $\hat{C}_{\mu,\nu}(1,1)$. For $\mu, \nu \approx 0$, the phase velocity is approximately 2; thus smooth waves propagate at a speed of 2 on the coarse grid. Moreover, as μ, ν increases, the phase velocity decreases from 2, suggesting that dispersion also occurs in the 2D case.

As an example, we solve the model entering flow problem by multigrid, and snapshots of the errors in the first 15 V-cycles are shown in Figure 4.2. We use bilinear interpolation, one presmoothing, and three grids. The mesh size is $h = 1/32$, and

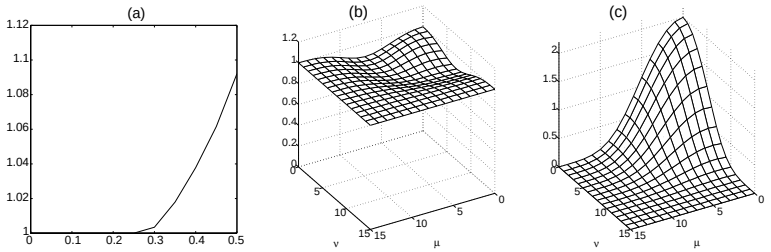

FIG. 4.1. *Spectrum of the Fourier transform of the inexact coarse grid correction for the entering flow problem.* (a) $\max_{\mu,\nu} |\hat{C}_{\mu,\nu}(1,1)|$ *with CFL-number* $0 \le \lambda \le 0.5$*;* (b) $|\hat{C}_{\mu,\nu}(1,1)|$, $\lambda = 0.25$*;* (c) *phase velocity of* $\hat{C}_{\mu,\nu}(1,1)$.

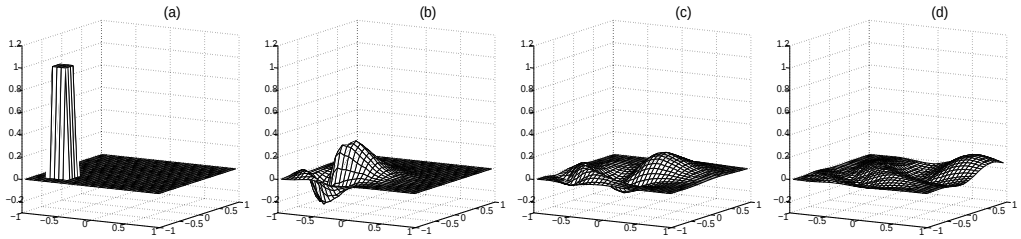

FIG. 4.2. *Numerical solutions given by a three-level multigrid for the entering flow problem at* (a) *iteration* $= 0$, (b) *iteration* $= 5$, (c) *iteration* $= 10$, (d) *iteration* $= 15$.

$\lambda = 0.25$. We observe that oscillations are generated at the tail as the square wave propagates from $(-1,-1)$ to (1,1), which agrees with our phase velocity analysis.

For the recirculating flow problem, Fourier analysis is not feasible, and yet we still observe a similar wave propagation phenomenon as in the entering flow case; see Figure 4.3. The same parameters are used as before. We can see that the wave rotates around the domain with oscillations at the tail due to dispersion of the coarse grid correction. Thus, the results of the phase velocity analysis for constant coefficient problems appear to hold also for variable coefficient problems.

4.2. Exact coarse grid solve, direct discretization CGO. Instead of applying a few steps of smoothing on the coarse grid, we solve the coarse grid equation exactly. Direct discretization is used for the CGO. Thus, the coarse grid correction matrix is

$$C = I - p(L^H)^{-1} r L^h,$$

and its Fourier transform is given by

$$\begin{aligned}\hat{C}_{\mu,\nu} &= I - \hat{p}_{\mu,\nu}(\hat{L}^H_{\mu,\nu})^{-1}\hat{r}_{\mu,\nu}\hat{L}^h_{\mu,\nu} \\ &= I - \begin{bmatrix} c_\mu^2 c_\nu^2 \\ -s_\mu^2 c_\nu^2 \\ -c_\mu^2 s_\nu^2 \\ s_\mu^2 s_\nu^2 \end{bmatrix} \frac{1}{\frac{a}{2h}(1 - e^{-\mu\pi 2hi}) + \frac{b}{2h}(1 - e^{-\nu\pi 2hi})} \\ &\quad \cdot \begin{bmatrix} c_\mu^2 c_\nu^2 & -s_\mu^2 c_\nu^2 & -c\mu^2 s_\nu^2 & s_\mu^2 s_\nu^2 \end{bmatrix} \hat{L}^h_{\mu,\nu}.\end{aligned}$$

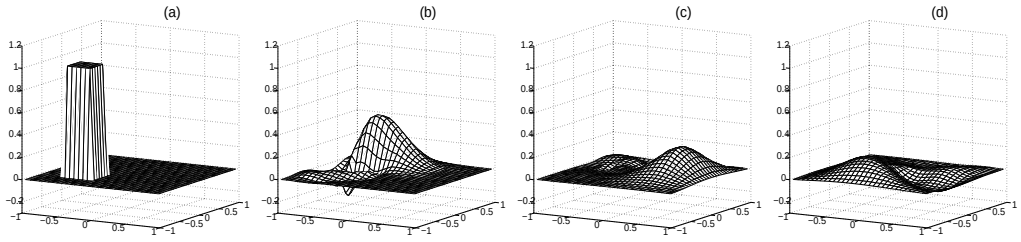

FIG. 4.3. *Numerical solutions given by a three-level multigrid for the recirculating flow problem at* (a) *iteration* = 0, (b) *iteration* = 5, (c) *iteration* = 10, (d) *iteration* = 15.

Therefore,

$$\hat{C}_{\mu,\nu}(1,1) = 1 - c_\mu^4 c_\nu^4 \frac{\frac{a}{h}(1-e^{-\mu\pi hi}) + \frac{b}{h}(1-e^{-\nu\pi hi})}{\frac{a}{2h}(1-e^{-\mu\pi 2hi}) + \frac{b}{2h}(1-e^{-\nu\pi 2hi})}.$$

To better understand the formula, we consider two special and yet important cases: frequency components in the characteristic direction, i.e., (μ,ν) such that

$$b\mu - a\nu = 0,$$

and the cross-characteristic direction[1] [4, 11, 39], i.e., (μ,ν) such that

$$a\mu + b\nu = 0.$$

THEOREM 4.2. *For the components in the characteristic direction and assuming* $a = b$,

$$|\hat{C}_{\mu,\nu}(1,1)| = \frac{\mu\pi h}{2} + O(\mu\pi h)^2.$$

For the components in the cross-characteristic direction and positive constants a, b,

$$\lim_{\mu\to 0} \hat{C}_{\mu,\nu}(1,1) = \frac{1}{2}.$$

In particular, for $a = b$, *then* $\hat{C}_{\mu,\nu}(1,1) = 1 - c_\mu^6/2$.

Proof. As in the corresponding 1D case, we are also interested in the effect of the exact coarse grid solve, i.e., $D = p(L^H)^{-1} r L^h$, whose Fourier transform is given by

$$\hat{D}_{\mu,\nu}(1,1) = c_\mu^4 c_\nu^4 \frac{\frac{a}{h}(1-e^{-\mu\pi hi}) + \frac{b}{h}(1-e^{-\nu\pi hi})}{\frac{a}{2h}(1-e^{-\mu\pi 2hi}) + \frac{b}{2h}(1-e^{-\nu\pi 2hi})}.$$

In the characteristic direction, and $a = b$, then

$$\hat{D}_{\mu,\nu}(1,1) = c_\mu^8 \frac{2a(1-e^{-\mu\pi hi})}{a(1-e^{-2\mu\pi hi})} = c_\mu^7 e^{\frac{\mu\pi hi}{2}}.$$

As a result,

$$\hat{C}_{\mu,\nu}(1,1) = 1 - c_\mu^7 e^{\frac{\mu\pi hi}{2}} = 1 - c_\mu^8 - i s_\mu c_\mu^7.$$

[1] Brandt and Yavneh refer to these components as characteristic components.

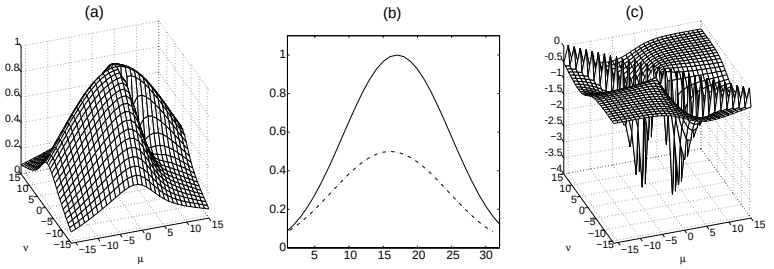

FIG. 4.4. *Spectrum of the Fourier transform of* $D = p(L^H)^{-1}rL^h$, *where* L^H *is obtained from the direct discretization of the entering flow problem.* (a) $|\hat{D}_{\mu,\nu}(1,1)|$; (b) $|\hat{D}_{\mu,\nu}(1,1)|$, $\mu = \nu$ *(solid line) and* $\mu = -\nu$ *(dashed line);* (c) *scaled phase angle of* $\hat{D}_{\mu,\nu}(1,1)$.

Then, we have $|\hat{C}_{\mu,\nu}(1,1)|^2 = 1 - 2c_\mu^8 + c_\mu^{14}$, and hence

$$|\hat{C}_{\mu,\nu}(1,1)| = \frac{\mu\pi h}{2} + O(\mu\pi h)^2.$$

In the cross-characteristic direction, and positive constants a, b, by l'Hospital's rule,

$$\begin{aligned}\lim_{\mu\to 0} \hat{C}_{\mu,\nu}(1,1) &= 1 - \lim_{\mu\to 0} \frac{2a(1-e^{-\mu\pi hi}) + 2b(1-e^{(a/b)\mu\pi hi})}{a(1-e^{-2\mu\pi hi}) + b(1-e^{2(a/b)\mu\pi hi})} \\ &= 1 - \lim_{\mu\to 0} \frac{2a(\pi hi)e^{-\mu\pi hi} - 2a(\pi hi)e^{(a/b)\mu\pi hi}}{2a(\pi hi)e^{-2\mu\pi hi} - 2a(\pi hi)e^{2(a/b)\mu\pi hi}} \\ &= \frac{1}{2}.\end{aligned}$$

For $a = b = 1$, the explicit formula for $\hat{C}_{\mu,\nu}(1,1)$ follows from direct substitution. □

We note that our analysis for the cross-characteristic direction is consistent with the result of Brandt and Yavneh [11] in which they also showed that $\lim_{\mu\to 0} \hat{C}_{\mu,\nu}(1,1) = 1/2$ for the special case $b = 0$, and so they concluded that the coarse grid error is not a good approximation to the fine grid error for components in the cross-characteristic directions. In [39], Yavneh proposes the use of higher order interpolation and restriction operators and more accurate discretizations of the CGO to improve the accuracy of the coarse grid correction.

In both [11, 39], the phase error is not discussed, which has been shown by Theorem 4.2 to be relevant for components in the characteristic direction. Specifically, in the characteristic direction, the magnitude of these components is accurate: $|\hat{D}_{\mu,\nu}(1,1)| = c_\mu^7$, $\mu \approx 0$. However, it has a phase error of $\mu\pi h/2$. Qualitatively speaking, the coarse grid error is shifted by $h/2$ in the characteristic direction, and hence the accuracy of $\hat{C}_{\mu,\nu}(1,1)$ is only first order.

Figure 4.4(a) shows that $|\hat{D}_{\mu,\nu}(1,1)| \approx 1$, for $\mu, \nu \approx 0$ and having the same sign, but is significantly below 1 for other values of μ and ν. In Figure 4.4(b), we plot the values of $|\hat{D}_{\mu,\nu}(1,1)|$ for $\mu = \nu$ (solid line) and $\mu = -\nu$ (dashed line). Both agree with the results of Theorem 4.2. Figure 4.4(c) shows the scaled values of the phase angles, $\frac{\theta}{(\mu+\nu)\pi h}$, which measure the amount of shift in the coarse grid error along the flow direction. In the characteristic direction, the amount of shift is negative and relatively constant. In the cross-characteristic direction, the amount of shift varies. Thus, we expect the coarse grid error to be slightly shifted from the fine grid error.

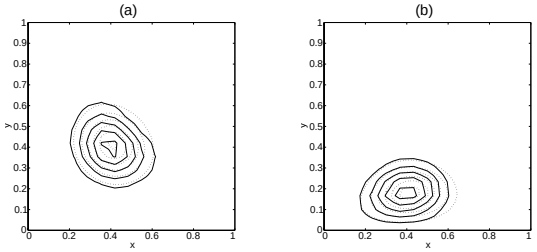

FIG. 4.5. *Contour plots of the fine grid error (dashed line) and the interpolated coarse grid error (solid line) for* (a) *the entering flow, and* (b) *the recirculating flow,.*

Figures 4.5(a) and (b) show the contour plots of the fine grid error (dashed line) and the interpolated coarse grid error (solid line) for the entering flow and recirculating flow, respectively. Both results agree with the phase analysis in that the interpolated coarse grid errors are shifted behind the direction of the flow. We note that the amount of shift depends on the mesh size, and hence it becomes more serious on the coarser meshes which occurs when many levels of multigrid are used.

4.3. Exact coarse grid solve, Galerkin CGO. To avoid the shifting phenomenon, we use the Galerkin approach to form the CGO, i.e.,

$$G^H = rL^h p.$$

Thus, the Fourier transform of the coarse grid correction matrix is given by

$$\hat{C}_{\mu,\nu} = I - \hat{p}_{\mu,\nu}(\hat{G}^H_{\mu,\nu})^{-1}\hat{r}_{\mu,\nu}\hat{L}^h_{\mu,\nu}.$$

We again consider the characteristic and cross-characteristic components.

THEOREM 4.3. *For the components in the characteristic direction and assuming constant* $a = b$,

$$|\hat{C}_{\mu,\nu}(1,1)| = \frac{(\mu\pi h)^3}{8} + O(\mu\pi h)^5.$$

For the components in the cross-characteristic direction and positive constants a, b,

$$\lim_{\mu\to 0} \hat{C}_{\mu,\nu}(1,1) = 0.$$

In particular, if $a = b$, *then*

$$|\hat{C}_{\mu,\nu}(1,1)| = \frac{(\mu\pi h)^2}{4} + O(\mu\pi h)^4.$$

Proof. First, consider $D = p(G^H)^{-1}rL^h$. Fourier transform gives

$$\hat{D}_{\mu,\nu}(1,1) = c_\mu^4 c_\nu^4 \frac{\hat{L}^h_{\mu,\nu}(1,1)}{\hat{G}^H_{\mu,\nu}}, \tag{4.1}$$

where the Fourier transform of the Galerkin CGO is given by

$$\begin{aligned}\hat{G}^H_{\mu,\nu} = {} & c_\mu^4 c_\nu^4 \left[\frac{a}{h}(1-e^{-\mu\pi hi}) + \frac{b}{h}(1-e^{-\nu\pi hi})\right] + s_\mu^4 c_\nu^4 \left[\frac{a}{h}(1+e^{-\mu\pi hi}) + \frac{b}{h}(1-e^{-\nu\pi hi})\right] \\ & + c_\mu^4 s_\nu^4 \left[\frac{a}{h}(1-e^{-\mu\pi hi}) + \frac{b}{h}(1+e^{-\nu\pi hi})\right] + s_\mu^4 s_\nu^4 \left[\frac{a}{h}(1+e^{-\mu\pi hi}) + \frac{b}{h}(1+e^{-\nu\pi hi})\right].\end{aligned}$$

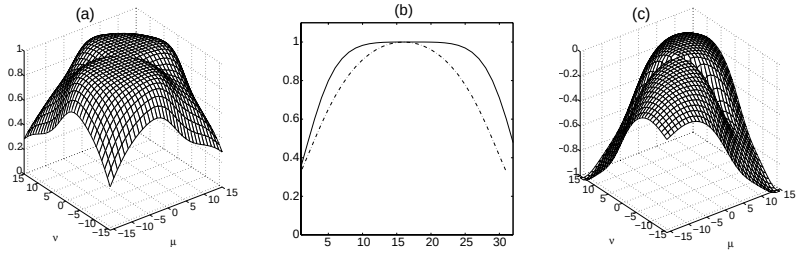

FIG. 4.6. *Spectrum of the Fourier transform of* $D = p(G^H)^{-1}rL^h$, *where* G^H *is obtained from the Galerkin approach to the entering flow problem.* (a) $|\hat{D}_{\mu,\nu}(1,1)|$, (b) $|\hat{D}_{\mu,\nu}(1,1)|$, $\mu = \nu$ *(solid line) and* $\mu = -\nu$ *(dashed line)* (c) *Scaled phase angle of* $\hat{D}_{\mu,\nu}(1,1)$.

In the characteristic direction and $a = b$, (4.1) becomes

$$\hat{D}_{\mu,\nu}(1,1) = \frac{c_\mu^7}{(c_\mu^4 + s_\mu^4)(c_\mu^6 + s_\mu^6)}(c_\mu^3 + is_\mu^3).$$

Let $\hat{D}_{\mu,\nu}(1,1) = |\hat{D}_{\mu,\nu}(1,1)|e^{i\theta}$ and, by direct calculation,

$$|\hat{D}_{\mu,\nu}(1,1)| = \frac{c_\mu^7}{(c_\mu^4 + s_\mu^4)\sqrt{c_\mu^6 + s_\mu^6}},$$
$$\theta = \frac{1}{8}(\mu\pi h)^3 + O(\mu\pi h)^5.$$

Thus, the coarse grid error is accurate in magnitude and the phase shift is negligibly small. As a result, we have

$$\hat{C}_{\mu,\nu}(1,1) = 1 - \hat{D}_{\mu,\nu}(1,1) = \frac{c_\mu^4 s_\mu^4 + s_\mu^{10} - is_\mu^3 c_\mu^7}{(c_\mu^4 + s_\mu^4)(c_\mu^6 + s_\mu^6)},$$

and the result follows from Taylor expansion.

In the cross-characteristic directions, general positive constants a, b, we obtain the limit result by a similar calculation as in the proof of Theorem 4.2. Finally, if in addition, $a = b$, then

$$\hat{C}_{\mu,\nu}(1,1) = 1 - \frac{c_\mu^2 s_\mu^2 + s_\mu^6}{c_\mu^6 + c_\mu^2 s_\mu^2 + s_\mu^6} = \frac{(\mu\pi h)^2}{4} + O(\mu\pi h)^4. \qquad \square$$

In the Galerkin approach, the magnitudes of smooth coarse grid errors are 1 for both cross-characteristic and characteristic components. Furthermore, there is essentially no phase shift in both directions, as opposed to the non-Galerkin approach. As a result, the coarse grid correction is second and third order accurate in the characteristic and cross-characteristic components, respectively.

Figure 4.6(a) shows that $|\hat{D}_{\mu,\nu}(1,1)| \approx 1$ for $\mu, \nu \approx 0$ in all directions. In particular, Figure 4.6(b) shows the values of $|\hat{D}_{\mu,\nu}(1,1)|$ in the characteristic (solid line) and cross-characteristic directions (dashed line), which verify the results of Theorem 4.3. Figure 4.6(c) shows the scaled values of the phase angles, $\frac{\theta}{(\mu+\nu)\pi h}$. Again for $\mu, \nu \approx 0$ in all directions, there is essentially no phase error.

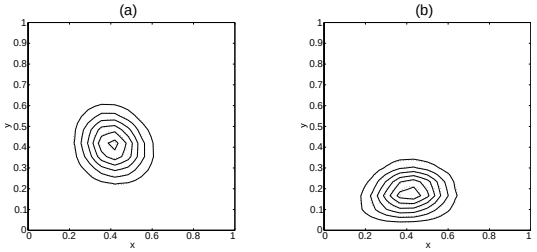

FIG. 4.7. *Contour plots of the fine grid error (dashed line) and the interpolated coarse grid error (solid line) for* (a) *the entering flow and* (b) *the recirculating flow.*

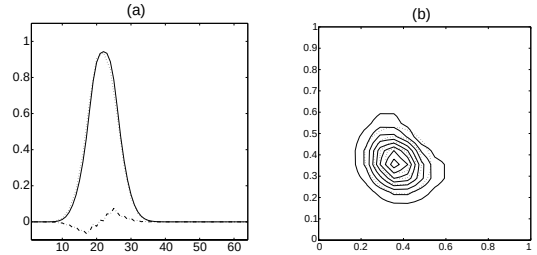

FIG. 4.8. (a) *Plots of the fine grid error (solid line), the coarse grid error (dotted line), and the error after coarse grid correction (dash-dotted line).* (b) *Contour plots of the fine grid error (dotted line) and the coarse grid error (solid line).*

Figures 4.7(a) and (b) show the contour plots of the fine grid error (dashed line) and the interpolated coarse grid error (solid line) for the entering flow and recirculating flow problems, respectively. Both results agree with the phase analysis in that the interpolated coarse grid errors match accurately with the fine grid errors.

4.4. High order method. We have considered first order upwind discretization so far. However, the phase error analysis is not restricted to first order methods. In fact, our phase error analysis does not assume any particular discretization schemes or multigrid methods. Here, we illustrate the phase shift error (cf. sections 3.2 and 4.2) for a second order total variation diminishing (TVD) scheme [25]:

$$u_x(x_i) \approx \frac{1}{h}\left(\left(u_i + \frac{1-\lambda}{2}s_i\right) - \left(u_{i-1} + \frac{1-\lambda}{2}s_{i-1}\right)\right),$$

where λ is a parameter (which in the time dependent case is the CFL-number) and $s_i = \text{minmod}(u_{i+1}-u_i, u_i-u_{i-1})$ is the minmod function. Since it is nonlinear, Fourier analysis is not applicable. Thus, we demonstrate the phase shift error numerically. The CGO is obtained by direct discretization and the coarse grid problem is solved exactly. In Figure 4.8(a), we show the fine grid error (solid line) and the error after coarse grid correction (dashed line). We can see that the coarse grid error is shifted to the left (probably by half a grid point), just like in Figure 3.2. The errors of the 2D entering flow problem are shown in Figure 4.8(b), where the contour plots of the fine grid error (dotted line) and the coarse grid error (solid line) are shown. As in Figure 4.5, the coarse grid error is shifted behind the direction of the flow. In conclusion, the phase error property of the coarse grid correction approach with the direct discretization CGO and exact coarse grid solve using the second order TVD schemes in one and two dimensions is consistent with the results using the first order upwind schemes.

4.5. Summary. In practice, the wave propagation approach is appealing since it is simple and uses the same smoothing method on all the coarse grids. However, such coarse grid correction is dispersive and oscillations generated can slow down multigrid convergence. For the exact coarse grid solve, direct discretization approach, the same smoothing method can also be used on all the coarse grids. Since exact coarse grid solve is used, the dispersive effect is much improved. However, the coarse grid correction is only first order accurate, leading to slower convergence. For the Galerkin approach, the coarse grid correction is more accurate, and hence the resulting multigrid convergence should be like the elliptic case.

We note that although our analysis suggests that the Galerkin approach has the least phase error, in practice, however, there are several issues to be addressed. It has been observed that the Galerkin CGOs on the coarse grids become more and more like the central finite difference operators and hence lead to stability problems. To remedy this, carefully designed interpolation and restriction are needed, for instance, operator-dependent interpolations and restrictions [14, 40], such that the resulting Galerkin CGO is stable. If the intergrid transfer operators are chosen such that the Galerkin CGO coincides with the one by direct discretization, then we would expect the phase error to be small even if direct discretization were used together with such intergrid transfer operators. The construction of an appropriate interpolation and restriction, however, requires further research.

5. Applications. In the FDA analysis [4, 10, 11], the effect of the interpolation and restriction operators are ignored. However, as we have seen, the phase error property of the coarse grid correction process is coupled with the CGO as well as the intergrid transfer operators. In this section, we show that the phase error analysis can explain the fast convergence of two multigrid methods which use direct discretization CGO and upwind-type interpolation and restriction.

5.1. Modified inexact coarse grid solve, direct discretization CGO. In section 3.1, we show that the convergence of the multigrid methods based on the wave propagation approach is slowed down by the dispersion effect. To fix this problem, upwind-type interpolation and restriction are proposed in [22]. More precisely, the upwind-biased residual restriction operator, r, can be defined as

$$r(d_i^h) = \frac{1}{2}(d_i^h + d_{i-1}^h), \tag{5.1}$$

where d^h is the fine grid residual. Similarly, the interpolation of a coarse grid function v^H is given by

$$(pv^H)_{2i} = (pv^H)_{2i+1} = v_{2i}^H.$$

Moreover, the coarse grid update formula is also modified:

$$u^{n+1} = \bar{u}^h + p(\bar{u}^H - ru^n),$$

where $\bar{u}^h$ and $\bar{u}^H$ are the approximate solutions after smoothing on the fine and coarse grids, respectively. When applying this multigrid method to solve the 1D problem, the iteration matrix M of a two-level method is given by

$$M = [I + p_{odd}r - \lambda(p_{even} + p_{odd})L^H r](I - \lambda L^h) - p_{odd}r,$$

where

$$p_{odd} = \begin{bmatrix} 0 & & & \\ 1 & & & \\ & 0 & & \\ & 1 & & \\ & & \ddots & \end{bmatrix}, \qquad p_{even} = \begin{bmatrix} 1 & & & \\ 0 & & & \\ & 1 & & \\ & 0 & & \\ & & \ddots & \end{bmatrix}, \qquad r = p_{even}^T.$$

In this case, the iteration matrix cannot be written as a product of two matrices. Thus, we will compute the eigenvalues of $\hat{M}$ directly.

LEMMA 5.1. *The Fourier transformed iteration matrix is given by*

$$\hat{M}_\mu = [I + (\hat{p}_{odd})_\mu(\hat{r})_\mu - \lambda((\hat{p}_{odd})_\mu + (\hat{p}_{even})_\mu)\hat{L}_\mu^H(\hat{r})_\mu](I - \lambda\hat{L}_\mu^h) - (\hat{p}_{odd})_\mu(\hat{r})_\mu,$$

where

$$(\hat{p}_{even})_\mu = \frac{1}{\sqrt{2}}\begin{bmatrix} e^{-\mu\pi hi} \\ e^{-\mu\pi hi} \end{bmatrix}, \qquad (\hat{p}_{odd})_\mu = \frac{1}{\sqrt{2}}\begin{bmatrix} 1 \\ -1 \end{bmatrix}, \qquad (\hat{r})_\mu = (\hat{p}_{even})_\mu^T.$$

Suppose the largest time step size is taken, i.e., $\lambda = 1.0$. We have the following result.

THEOREM 5.2. *The eigenvalues of $\hat{M}_\mu$ are* 0 *and $e^{-4\mu\pi hi}$.*

Proof. Simplifying the formula for $\hat{M}_\mu$ in Lemma 5.1 with $\lambda = 1.0$, we obtain

$$\hat{M}_\mu = e^{-3.5\mu\pi hi}\begin{bmatrix} \cos(\mu\pi h/2) & -\cos(\mu\pi h/2) \\ i\sin(\mu\pi h/2) & -i\sin(\mu\pi h/2) \end{bmatrix}.$$

By direct calculation, the eigenvalues of $\hat{M}_\mu$ are 0 and $e^{-4\mu\pi hi}$. ∎

By Theorem 5.2, the phase velocity is 4 for any wave number μ. Hence there is no dispersion, as opposed to the wave propagation approach discussed in section 3.1. In other words, the numerical error will propagate with a speed of 4. Numerical results showing fast convergence of this multigrid method can be found in [22].

5.2. Modified exact coarse grid solve, direct discretization CGO. Linear interpolation and full weighting are used in the exact coarse grid correction, direct discretization approach in section 3.2. Here we use the upwind restriction defined in (5.1) instead. For an analysis that ignores the interpolation and restriction operators used, for instance, the first differential approximate analysis [4], we would have concluded that the modified multigrid method would not be any better than the one using full weighting. However, as indicated in the numerical section of [4, p. 84], such restriction indeed leads to better convergence, but no explanation was given. We can explain this phenomenon from the phase velocity perspective. In particular, we shall show that there can be no phase error in the coarse grid correction.

THEOREM 5.3. *The* $(1,1)$ *entry of the Fourier transformed coarse grid correction matrix is*

$$\hat{C}_\mu(1,1) = s_\mu^2.$$

Proof. Denote the upwind restriction operator by $\tilde{r}$. Using the Fourier transform results in sections 3.2 and 5.1, the Fourier transform of the coarse grid correction

TABLE 6.1

Number of two-grid V-cycles for the 1D linear wave equation using inexact coarse grid solve, direct discretization (inexact), exact coarse grid solve, direct discretization (non-Galerkin), and exact coarse grid solve, Galerkin CGO (Galerkin).

h	Inexact	Non-Galerkin	Galerkin
1/32	31 (35)	13 (16)	8 (11)
1/64	44 (52)	9 (16)	5 (12)
1/128	73 (83)	6 (17)	3 (12)
1/256	141 (144)	5 (17)	3 (12)

matrix is given by

$$\begin{aligned}\hat{C}_\mu &= I - \hat{p}_\mu (\hat{L}_\mu^H)^{-1} \hat{\hat{r}}_\mu \hat{L}^h \\ &= I - \sqrt{2} \begin{bmatrix} c_\mu^2 \\ -s_\mu^2 \end{bmatrix} \frac{2h}{1 - e^{-2\mu\pi hi}} \frac{1}{2\sqrt{2}} \begin{bmatrix} e^{-\mu\pi hi} + 1 & e^{-\mu\pi hi} - 1 \end{bmatrix} \\ &\quad \cdot \frac{1}{h} \begin{bmatrix} 1 - e^{-\mu\pi hi} & 0 \\ 0 & 1 + e^{-\mu\pi hi} \end{bmatrix} \\ &= \begin{bmatrix} s_\mu^2 & c_\mu^2 \\ s_\mu^2 & c_\mu^2 \end{bmatrix}. \qquad \square\end{aligned}$$

As opposed to the results in section 3.2, if appropriate interpolation and/or restriction is used, there is no phase error in the coarse grid correction process when direct discretization is used. Hence, fast multigrid convergence is expected. In fact, the Fourier transformed coarse grid correction matrix coincides with the one derived in the case of the Poisson equation.

6. Numerical results. In the following, we compare the effects of different coarse grid corrections on the convergence of multigrid V-cycles. The first example is the steady state solution of the 1D linear wave equation:

$$u_t + u_x = 0.$$

Euler's method is used as the smoother for the approaches with CFL number $\lambda = 0.5$. Linear interpolation and full weighting restriction are used between grids. The multigrid V-cycle iterations stop when the relative residual norm is less than 10^{-6}. Zero boundary condition is used.

The number of multigrid V-cycles is shown in Table 6.1. For simplicity, we denote the three coarse grid correction approaches by *inexact, non-Galerkin,* and *Galerkin*, respectively. To verify the results of the previous sections, we use two multigrid levels and consider a smooth initial guess and a square wave initial guess (in parentheses). The results show that the number of multigrid V-cycles taken by the inexact coarse grid correction increases as the mesh size decreases; thus we do not observe the classical mesh-independent convergence. Moreover, the convergence is slow due to the dispersion of the inexact coarse grid solve. Both non-Galerkin and Galerkin approaches, which use exact coarse grid solve, show much better convergence. However, due to the phase error that occurred at coarse grid correction, the non-Galerkin approach is not as efficient as the Galerkin approach. We also note that the square wave initial guess, which consists of more significant intermediate high frequencies, has more severe dispersive effects on the multigrid convergence. Qualitatively speaking, both initial guesses give very similar results and hence we will show only those using the smooth initial guess in the following tests.

TABLE 6.2
Number of multigrid V-cycles with 2 *to* 6 *number of coarse grids for the* 1*D linear wave equation using inexact and non-Galerkin coarse grid corrections.*

	Inexact					Non-Galerkin				
h	2	3	4	5	6	2	3	4	5	6
1/32	31	35	39			13	25	34		
1/64	44	43	45	51		9	22	37	46	
1/128	73	52	58	61	61	6	13	31	49	55
1/256	141	83	64	72	72	5	9	19	40	59

TABLE 6.3
Number of two-grid V-cycles for the 2*D entering and recirculating flow problems using inexact, non-Galerkin, and Galerkin coarse grid corrections.*

	Entering flow			Recirculating flow		
h	Inexact	Non-Galerkin	Galerkin	Inexact	Non-Galerkin	Galerkin
1/32	28	13	7	63	14	6
1/64	41	13	5	72	14	6
1/128	70	11	5	84	14	7
1/256	134	9	5	> 100	14	8

The same qualitative results hold when more coarse grids are used. Table 6.2 shows the multilevel convergence of the inexact and non-Galerkin coarse grid correction approaches. The Galerkin approach requires different smoothing parameters on the coarse grids since the CGOs are changed from grid to grid, and hence it is not tested in this case. For the inexact coarse grid correction approach, the convergence should, in principle, have been improved by using more coarse grids based on the result of Gustafsson and Lötstedt (cf. Theorem 2.1). This is indeed true when the mesh size is very small ($h = 1/256$) since the small wave number components are more dominant in the initial guess. But when the coarse grid becomes smaller, the convergence starts to deteriorate. For the non-Galerkin approach, the multigrid convergence also starts to deteriorate on the coarser grids due to the shift of the coarse grid errors, which is more serious with larger mesh size. Thus the phase errors in the coarse grid correction cause more serious damage to the multigrid convergence with more coarse grid levels.

We next consider the model entering flow and recirculating flow problems in two dimensions (cf. section 4). For the entering flow problem, two pre- and two post-Euler's smoothing are used for all the coarse grid correction approaches and the CFL number, $\lambda = 0.25$. For the recirculating flow problem, we find that the smoothing effect of Euler's method is very poor. Thus, we use Gauss–Seidel for the presmoothing and backward Gauss–Seidel for the postsmoothing. As noted in section 4, special orderings are often used to enhance convergence. But here, we focus on the coarse grid correction part, and therefore natural ordering is used. Linear interpolation and full weighting restriction are used for all cases except for the singular point (0.5,0.5) of the recirculating flow problem, in which injection is used instead [11].

The two-grid results are shown in Table 6.3. As in the 1D case, the convergence of the Runge–Kutta coarse grid correction approach is slow because of the dispersion effect. The convergence of the non-Galerkin and Galerkin approaches is shown to be insensitive to the mesh size. We also remark that although our phase velocity analysis cannot be applied to variable coefficient cases, the numerical results of the recirculating flow indicate that the same conclusions hold for the different coarse grid correction approaches.

We remark that the numerical results in Table 6.3 can be improved by using more robust smoothers [35], for instance, four direction point Gauss–Seidel, alternating line Jacobi with damping, and alternating zebra relaxation with damping. In this paper, however, we focus on the coarse grid correction and do not optimize the choice of smoothers.

7. Conclusions. We have demonstrated that phase error analysis is a useful tool for analyzing multigrid methods for convection dominated problems and brings more insight into the efficiency of different coarse grid correction approaches. In contrast with the elliptic case, where multigrid convergence is governed by smoothing of high frequencies and coarse grid correction of the smooth frequencies, we have shown that it also depends on the phase errors on coarse grids for hyperbolic problems.

For Runge–Kutta coarse grid correction, the propagation of smooth waves is accelerated by using coarse grids. However, dispersion occurs in the coarse grid correction process, which substantially slows down the multigrid convergence. The exact coarse grid solve approach does not rely on wave propagation, and hence dispersion is not an issue. However, for the use of the discretization matrix as the CGO, there is a phase shift error in the coarse grid error which deteriorates the multigrid convergence. The Galerkin approach has the advantage of maintaining small shift error in the coarse grid correction. However, one needs to form the CGOs on every grid, and hence to determine new sets of parameters, e.g., time step size, for the smoother to obtain good smoothing efficiency.

We have addressed the issue of phase error analysis of multigrid methods for convection dominated problems. However, the design of new multigrid methods which possess good phase error properties requires further investigation.

REFERENCES

[1] J. Bey and G. Wittum, *Downwind numbering: Robust multigrid for convection-diffusion problems*, Appl. Numer. Math., 23 (1997), pp. 177–192.

[2] J. Bramble, J. Pasciak, J. Wang, and J. Xu, *Convergence estimates for multigrid algorithms without regularity assumptions*, Math. Comp., 57 (1991), pp. 23–45.

[3] A. Brandt, *Multi-level adaptive solutions to boundary-value problems*, Math. Comp., 31 (1977), pp. 333–390.

[4] A. Brandt, *Multigrid Solvers for Non-Elliptic and Singular-Perturbation Steady-State Problems*, Tech. report, Department of Applied Mathematics, The Weizmann Institute of Science, Rehovot, Israel, 1981.

[5] A. Brandt, *Guide to multigrid development*, in Multigrid Methods, W. Hackbusch and U. Trottenberg, eds., Lectures Notes in Math. 960, Springer-Verlag, Berlin, 1982, pp. 220–312.

[6] A. Brandt, *Multigrid Techniques:* 1984 *Guide with Applications to Fluid Dynamics*, GMD–Studien Nr. 85, Gesellschaft für Mathematik und Datenverarbeitung, St. Augustin, 1984.

[7] A. Brandt, *Rigorous local mode analysis of multigrid*, in Preliminary Proceedings of the Fourth Copper Mountain Conference on Multigrid Methods, Vol. I, J. Mandel and S. F. McCormick, eds., Computational Mathematics Group, University of Colorado, Denver, CO, 1989, pp. 55–133.

[8] A. Brandt, *Rigorous quantitative analysis of multigrid*, I: *Constant coefficients two-level cycle with L_2-norm*, SIAM J. Numer. Anal., 31 (1994), pp. 1695–1730.

[9] A. Brandt, *Barriers to Achieving Textbook Multigrid Efficiency (TME) in CFD*, Tech. report, NASA/CR-1998-207647, IC NASA Center for AeroSpace Information (CASI), Hanover, MD, 1998.

[10] A. Brandt and I. Yavneh, *On multigrid solution of high-Reynolds incompressible entering flows*, J. Comput. Phys., 101 (1992), pp. 151–164.

[11] A. Brandt and I. Yavneh, *Accelerated multigrid convergence and high-Reynolds recirculating flows*, SIAM J. Sci. Comput., 14 (1993), pp. 607–626.

[12] T. F. Chan and W. L. Wan, *Robust multigrid methods for elliptic linear systems*, J. Comput. Appl. Math., 123 (2000), pp. 323–352.

[13] T. F. Chan and H. C. Elman, *Fourier analysis of iterative methods for elliptic boundary value problems*, SIAM Rev., 31 (1989), pp. 20–49.
[14] J. E. Dendy, Jr., *Black box multigrid for nonsymmetric problems*, Appl. Math. Comput., 13 (1983), pp. 261–283.
[15] B. Gustafsson and P. Lötstedt, *Analysis of the multigrid method applied to first order systems*, in Proceedings of the Fourth Copper Mountain Conference on Multigrid Methods, J. Mandel, S. F. McCormick, J. E. Dendy, Jr., C. Farhat, G. Lonsdale, S. V. Parter, J. W. Ruge, and K. Stüben, eds., SIAM, Philadelphia, 1989, pp. 181–233.
[16] W. Hackbusch, *Multigrid convergence for a singular perturbation problem*, Linear Algebra Appl., 58 (1984), pp. 125–145.
[17] W. Hackbusch, *Multigrid Methods and Applications*, Springer-Verlag, Berlin, 1985.
[18] W. Hackbusch and T. Probst, *Downwind Gauss-Seidel smoothing for convection dominated problems*, Numer. Linear Algebra Appl., 4 (1997), pp. 85–102.
[19] A. Jameson, *Solution of the Euler equations for two dimensional transonic flow by a multigrid method*, Appl. Math. Comput., 13 (1983), pp. 327–355.
[20] A. Jameson, *Computational transonics*, Comm. Pure Appl. Math., 41 (1988), pp. 507–549.
[21] A. Jameson, W. Schmidt, and E. Turkel, *Numerical Solutions of the Euler Equations by Finite Volume Methods Using Runge-Kutta Time-Stepping Schemes*, AIAA paper 81-1259, American Institute of Aeronautics and Astronautics, Reston, VA, 1981.
[22] A. Jameson and W. L. Wan, *Monotonicity Preserving and Total Variation Diminishing Multigrid Time Stepping Methods*, Tech. report CS-2001-11, Department of Computer Science, University of Waterloo, Waterloo, ON, Canada, 2001.
[23] D. C. Jespersen. *A Time-Accurate Multiple-Grid Algorithm*, AIAA paper 85-1493-CP, American Institute of Aeronautics and Astronautics, Reston, VA, 1985.
[24] K. Johannsen, *Robust Smoothers for Convection-Diffusion Problems*, Tech. report, Institute for Computer Applications, University of Stuttgart, Stuttgart, Germany, 1999.
[25] R. LeVeque, *Numerical Methods for Conservation Laws*, Birkhäuser, Zürich, 1992.
[26] P. Lötstedt and B. Gustafsson, *Fourier analysis of multigrid methods for general systems of PDEs*, Math. Comp., 60 (1993), pp. 473–493.
[27] R. H. Ni, *A multiple-grid scheme for solving the euler equations*, AIAA J., 20 (1982), pp. 1565–1571.
[28] A. Reusken, *Multigrid with matrix-dependent transfer operators for a singular perturbation problem*, Computing, 50 (1993), pp. 199–211.
[29] A. Reusken, *Fourier analysis of a robust multigrid method for two-dimensional convection-diffusion equations*, Numer. Math., 71 (1995), pp. 365–398.
[30] K. Stüben and U. Trottenberg, *Multigrid methods: Fundamental algorithms, model problem analysis and applications*, in Multigrid Methods, Proceedings, Köln-Porz, 1981, W. Hackbusch and U. Trottenberg, eds., Lecture Notes in Math. 960, Springer-Verlag, Berlin, 1982, pp. 1–176.
[31] U. Trottenberg, C. Oosterlee, and A. Schüller, *Multigrid*, Academic Press, New York, 2001.
[32] R. Vichnevetsky and J. B. Bowles, *Fourier Analysis of Numerical Approximations of Hyperbolic Equations*, Studies in Appl. Math. 5, SIAM, Philadelphia, 1982.
[33] W. L. Wan and T. F. Chan, *A Phase Velocity Analysis of Multigrid Methods for Hyperbolic Equations*, Tech. report CAM 02-24, Department of Mathematics, UCLA, Los Angeles, CA, 2002.
[34] F. Wang and J. Xu, *A crosswind block iterative method for convection-dominated problems*, SIAM J. Sci. Comput., 21 (1999), pp. 620–645.
[35] P. Wesseling, *An Introduction to Multigrid Methods*, Wiley, Chichester, UK, 1992.
[36] R. Wienands and C. W. Oosterlee, *On three-grid Fourier analysis for multigrid*, SIAM J. Sci. Comput., 23 (2001), pp. 651–671.
[37] J. Xu, *Iterative methods by space decomposition and subspace correction*, SIAM Rev., 34 (1992), pp. 581–613.
[38] N. N. Yanenko and Y. I. Shokin, *Correctness of first differential approximations of difference schemes*, Sov. Math. Dokl., 9 (1968), pp. 1215–1217.
[39] I. Yavneh, *Coarse-grid correction for nonelliptic and singular perturbation problems*, SIAM J. Sci. Comput., 19 (1998), pp. 1682–1699.
[40] P. M. De Zeeuw, *Matrix-dependent prolongations and restrictions in a blackbox multigrid solver*, J. Comput. Appl. Math., 33 (1990), pp. 1–27.